JOURNAL OF GEOPHYSICAL RESEARCH, VOL. 113, E00A08, doi:10.1029/2007JE003002, 2008



# Lidar on the Phoenix mission to Mars

James Whiteway,[1] Michael Daly,[2] Allan Carswell,[3] Thomas Duck,[4] Cameron Dickinson,[1] Leonce Komguem,[1] and Clive Cook[1]

Received 30 August 2007; revised 9 March 2008; accepted 5 May 2008; published 15 July 2008.

[1] A lidar system for atmospheric measurements will operate from the surface of Mars as part of the Phoenix mission. This will measure the height profile of backscattered laser light from airborne dust and clouds. These observations will be coordinated with solar radiation measurements and in situ sampling to study the climate and the water cycle. The design and testing of the lidar system are described, and measurements are presented that demonstrate the analysis methods and the performance characteristics.

**Citation:** Whiteway, J., M. Daly, A. Carswell, T. Duck, C. Dickinson, L. Komguem, and C. Cook (2008), Lidar on the Phoenix mission to Mars, *J. Geophys. Res.*, *113*, E00A08, doi:10.1029/2007JE003002.

## 1. Introduction

[2] The Phoenix mission will land on the north polar region of Mars on 25 May 2008 and operate for at least 90 sols. A description of the overall mission is provided by *Smith et al.* [2008]. The atmospheric component of the mission will advance our knowledge of the climate on Mars by combining lidar remote sensing of atmospheric dust and clouds with measurements of solar radiation (M. Lemmon et al., The Phoenix Surface Stereo Imager (SSI) investigation, manuscript in preparation, 2008) and in situ sampling of temperature, pressure, wind [*Taylor et al.*, 2008], and water vapor (A. P. Zent et al., The Thermal Electrical Conductivity Probe for Phoenix, submitted to *Journal of Geophysical Research*, 2008).

[3] The day to day variation of the local weather on Mars is controlled primarily by the amount of solar radiation reaching the surface and this depends on the optical thickness of the dust suspended in the atmosphere. This affects local and global meteorological patterns which in turn determine the lifting of dust from the surface and long-range transport [*Leovy*, 2001; *Newman et al.*, 2002]. There is also a climate interaction with the distribution of water ice above and below the surface of Mars [*Boynton et al.*, 2002; *Pathak et al.*, 2008]. This involves transport of water through the atmosphere and previous measurements from orbit have indicated that clouds could play a substantial role [*Clancy et al.*, 1996; *Neumann et al.*, 2003].

[4] The lidar on the Phoenix mission will record the height profile of laser backscatter from the dust and cloud layers that drift past the landing site. The lidar signal can be used to derive the optical extinction coefficient and this is critical for understanding the weather and climate. The absorption and scattering of solar radiation by dust has a first-order effect on heating of the atmosphere and surface. The derived optical extinction coefficient can also be related to the amount of scattering material. For example, the extinction coefficient derived from a lidar backscatter signal can be used to estimate the ice water content within a thin cloud [*Heymsfield et al.*, 2005]. Lidar cloud measurements will be of vital importance to the mission goal to investigate water on Mars. The combination of the lidar and passive remote sensing with in situ sampling will provide a view of the interacting processes that determine the local weather at the surface and also the role of the atmosphere in the water cycle on Mars.

## 2. Lidar Instrument

[5] A basic lidar (light detection and ranging) emits pulses of laser light into the atmosphere and then it detects and records the backscattered light as a function of time [*Measures*, 1984]. The time resolved signal is converted to distance using the speed of light. The Phoenix lidar operates in this manner with the characteristics listed in Table 1. A schematic diagram is shown in Figure 1, and a photograph of the system with the cover removed is shown in Figure 2.

[6] A drawing of the lidar transmitter assembly is shown in Figure 3. It is based on a diode pumped, passively Q-switched, neodymium-doped yttrium aluminum garnet (Nd:YAG) laser. This configuration was chosen for its robustness and technological maturity as much as for its suitable lidar performance. The pump diode array emits at a wavelength of 808 nm and is used to provide the energy to the Nd:YAG crystal within the laser cavity. Lasing is inhibited within the cavity through the use of a saturable absorber (a passive Q switch). The photon density within the oscillator cavity builds to a level where the saturable absorber bleaches and the energy within the cavity is dumped as a laser pulse over a very short time. For this laser the output light pulse has a length of 10 ns and an energy of 0.7 mJ.

[7] After the laser cavity emits a light pulse, part of the optical energy is converted from a wavelength of 1064 nm

[1]Department of Earth and Space Science and Engineering, York University, Toronto, Ontario, Canada.
[2]MDA Space Missions, Brampton, Ontario, Canada.
[3]Optech Inc., Vaughan, Ontario, Canada.
[4]Department of Physics and Atmospheric Science, Dalhousie University, Halifax, Nova Scotia, Canada.


0148-0227/08/2007JE003002$09.00

**Table 1.** Basic Characteristics of the Phoenix Lidar

| | 1064 nm | 532 nm |
|---|---|---|
| | *Transmitter* | |
| Laser | Nd: YAG Diode pumped | |
| Wavelengths | 1064 nm | 532 nm |
| Pulse repetition rate | 100 Hz | 100 Hz |
| Pulse energy | 0.3 mJ | 0.4 mJ |
| Divergence | 0.25 mrad | 0.25 mrad |
| Emitted line width | 0.25 nm | 0.25 nm |
| | *Receiver* | |
| Telescope | 10 cm diameter | |
| Field of View | 2 mrad | 1.5 mrad |
| Spectral width | 2 nm | 1 nm |
| Detector | Silicon APD | PMT |
| Signal recording | Analog:14 bit ADC | Analog: 14 bit ADC + Photon Counting |
| Sampling frequency | 30 MHz (5 m) | 30 MHz (5 m) |
| Total mass | 6 kg | |
| Maximum power | 30 W | |

to 532 nm by second harmonic generation in a potassium titanyl phosphate (KTP) crystal. The laser output is then expanded by a factor of 10 in order to reduce the divergence to 0.5 mrad. A small fraction of the outgoing laser pulse is "picked off" and separated into the two wavelength components in order to measure the relative amplitude of each wavelength with photodiodes. The signal from the photodiode detecting the 1064 nm pulse is used to trigger the data acquisition electronics, providing a zero-time reference, and also to shut off the pumping diodes.

[8] Figure 1 shows how the backscatter signals are collected by an afocal reflective telescope and split into the two relevant wavelengths using a dichroic mirror. The 1064 nm backscatter is detected by an avalanche photodiode (APD), and recorded using 14-bit analog to digital conversion (ADC). The 532 nm backscatter is detected by a photomultiplier (PMT) and the signal is recorded using both ADC and photon counting. Photon counting is required to record the weak signals from heights above 5 km and up to 20 km.

[9] The signal as a function of height is integrated over a set number of laser pulses and height bins. For example the standard operating mode is to use 50 m vertical resolution (ten 5 m bins summed) and 20 s temporal resolution (2000 laser pulses summed). These profiles are then stored sequentially. The temporal and spatial averaging parameters are part of the commands transmitted from the ground station during the mission.

## 3. Lidar System Testing

[10] Verification that the Phoenix lidar can function on Mars was achieved by operating it within a thermal vacuum (T-vac) chamber filled with $CO_2$ at a pressure of 8 torr and a temperature of $-70°C$. A window was installed in the T-vac chamber so that the output laser pulses and the receiver field of view could be directed across the "clean room" and through another window into the atmosphere in the zenith direction. Atmospheric observations could then be acquired and compared with simultaneous measurements provided by an independent lidar system.

[11] The lidar used for side-by-side comparison in testing was supplied by York University (referred to as the York Lidar). This has the same essential characteristics as the Phoenix lidar. For example, the transmitted wavelengths are the same (1064 nm and 532 nm), and the same detectors are applied in the receiver. The data acquisition electronics provide the same function as in the Phoenix lidar: analog

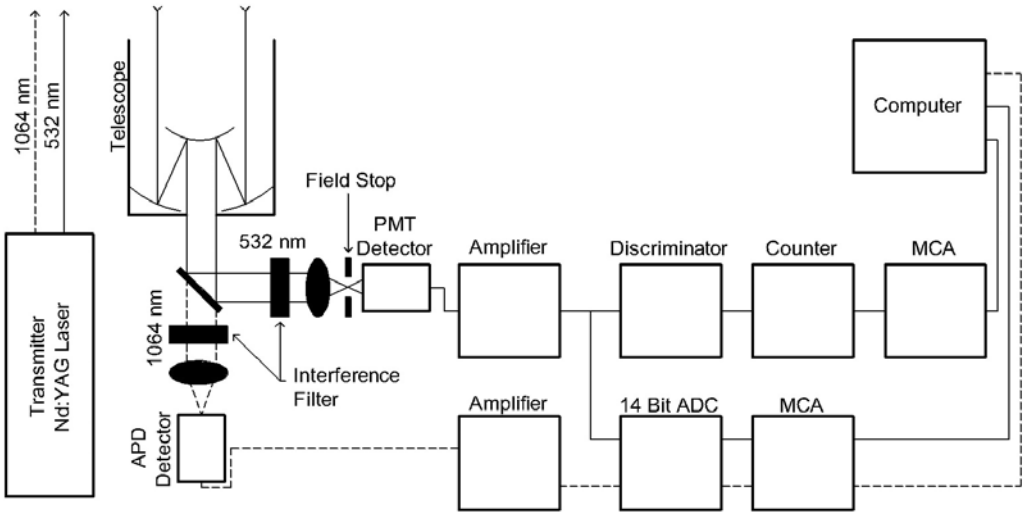


**Figure 1.** Schematic diagram of the Phoenix lidar.

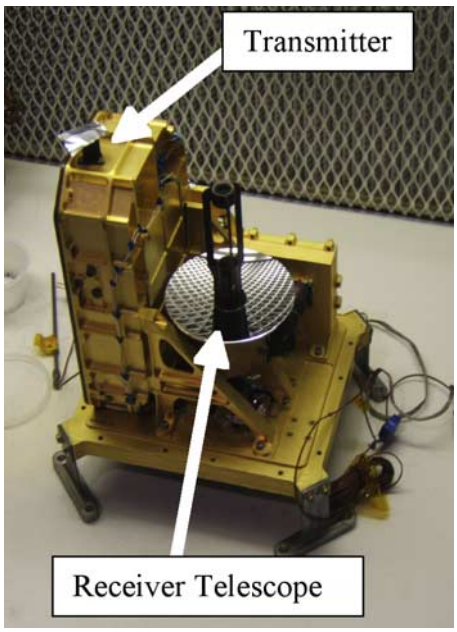


**Figure 2.** Photograph of the Phoenix lidar with the cover removed.

to digital conversion (ADC) at 1064 nm; both ADC and photon counting at 532 nm. The main difference is that the York Lidar has a more powerful laser than the Phoenix lidar.

[12] An important part of the testing was to ensure that the receiver and transmitter remain aligned over the full range of temperatures that are expected during the mission. The temperature within the lidar is controlled by heaters and the coldest it will get during the mission is −40°C. The heat dissipated by the laser while operating will increase the temperature of the instrument by about 3°C over a 15 min interval, depending on environmental conditions. The baseline plan is to have the lidar operate for four separate 15 min intervals at midday, evening, midnight, and morning. In this scenario the temperature of the lidar chassis is not expected to rise above −20°C. If the lidar is run for longer periods and more often, then the lidar chassis will get warmer. The alignment of the transmitter was optimized so that it was pointing within the receiver telescope FOV over a temperature range of −40°C to −10°C on the lidar chassis.

[13] The direction of the transmitted laser light relative to the receiver telescope field of view (FOV) was determined by deflecting the transmitted light with a variable optical wedge. The direction of the transmitted light was deflected until the atmospheric backscatter signal at a height of 1.5 km started to decrease and this was done in the four cardinal directions. The outline of the FOV could then be determined relative to the transmitter output. This was done at various temperatures between −40°C and 0°C. It was determined that the relative angle between the transmitted light pulse and the receiver telescope FOV axis changed by 0.9 mrad over the temperature range from −40°C to 0°C, moving inward toward the telescope axis as the temperature increased. The transmitted light pulse has a divergence of 0.5 mrad, so there is 1 mrad of tolerance within the 1.5 mrad FOV to account for temperature variations. Thus it was possible to optimize the alignment of the system so that the transmitter is pointing within the FOV over the range of temperature from −40°C to 0°C. This was done so that at −40°C the transmitter output is pointing 0.4 mrad away from the central axis of the receiver telescope FOV. It is still within the full 1.5 mrad of the FOV, with a 0.1 mrad tolerance between the outside edge of the transmitted laser pulse and the edge of the FOV. At a temperature of 0°C the transmitter was pointing 0.5 mrad toward the receiver telescope.

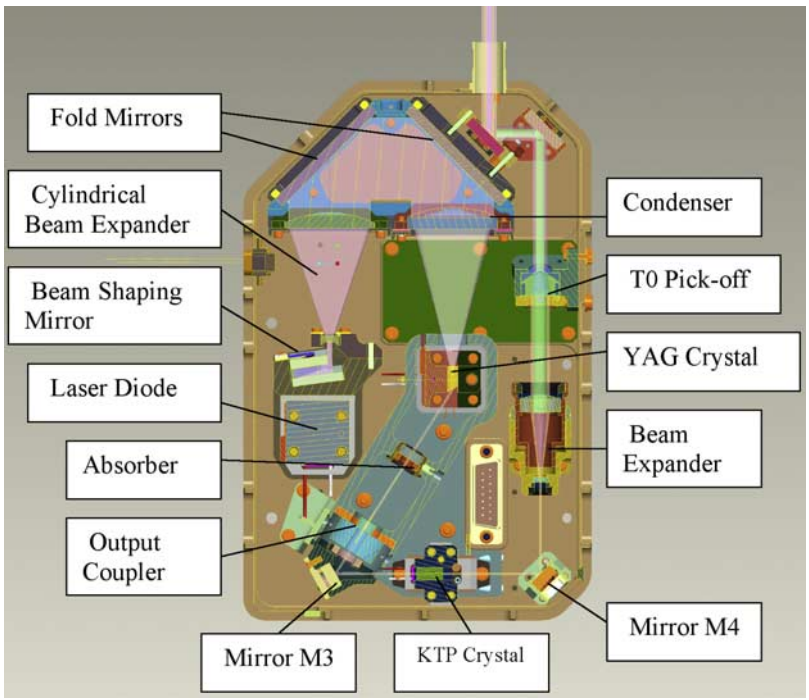


**Figure 3.** Drawing of the Phoenix lidar laser transmitter.

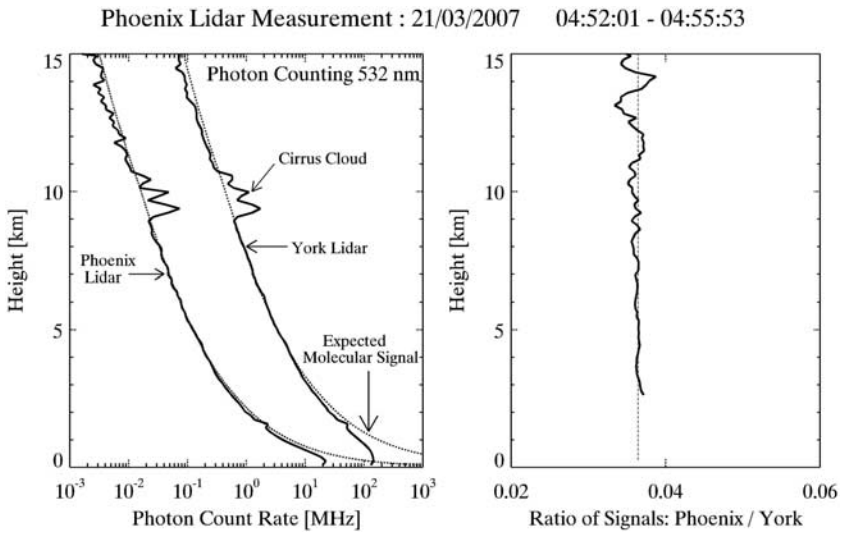


**Figure 4.** Atmospheric measurements obtained simultaneously with the Phoenix lidar and the York Lidar at the wavelength of 532 nm. The Phoenix lidar was operating inside the thermal vacuum chamber in an environment consisting of carbon dioxide at a pressure of 8 torr and a temperature of −70°C. The Phoenix lidar internal chassis temperature was −36°C.

[14] The height above which the cross section of the outgoing laser pulse is contained within the telescope FOV depends on the relative angle between the transmitter and receiver, and this depends on temperature. The height for 95% overlap is 1.1 km at a temperature of −40°C and 150 m at −10°C. A temperature-dependent correction for the partial overlap at lower heights is included in the Phoenix Lidar Characterization Report that will be available within the archive on the Planetary Data System.

[15] The alignment of the Phoenix lidar in Mars conditions was verified by direct comparison to the York Lidar with simultaneous atmospheric measurements. An example of a comparison between the York lidar and Phoenix lidar with photon counting signal acquisition is shown in Figure 4. The Phoenix lidar was in the T-vac chamber with 8 torr of $CO_2$ at a temperature of −70°C, and the lidar chassis temperature was −36°C. The ratio of the signals from the two lidars is constant with height up to above 15 km, and this is an indication that the Phoenix lidar transmitter is aligned within the receiver field of view. Another indication that the system is properly aligned is in the comparison with the expected signal from molecular backscatter.

[16] There is an enhancement in the signals in Figure 4 between heights of 9 km and 11 km due to a cirrus cloud layer. There is also a thin cloud at a height of 1.5 km. It is

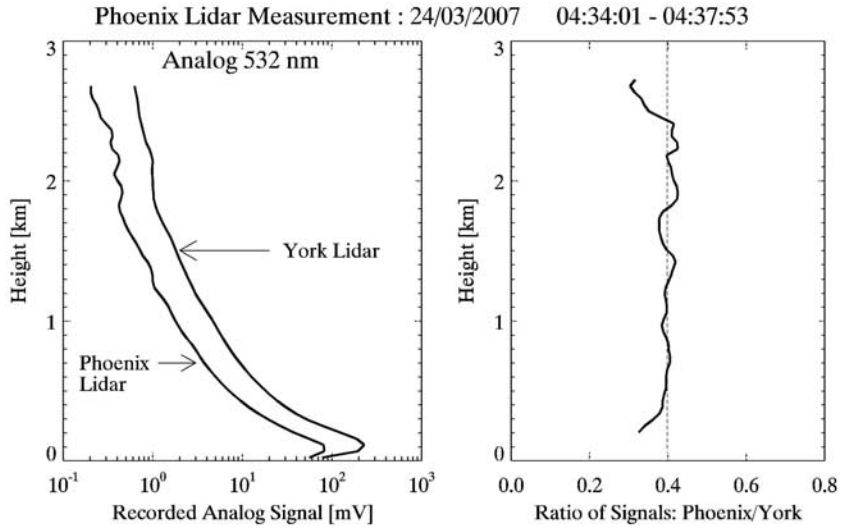


**Figure 5.** Atmospheric measurements obtained simultaneously with the Phoenix lidar and the York Lidar at the wavelength of 532 nm and recorded by analog to digital conversion. The Phoenix lidar was operating inside the thermal vacuum chamber in an environment consisting of carbon dioxide at a pressure of 8 torr and a temperature of −70°C. The Phoenix lidar internal chassis temperature was −30°C.

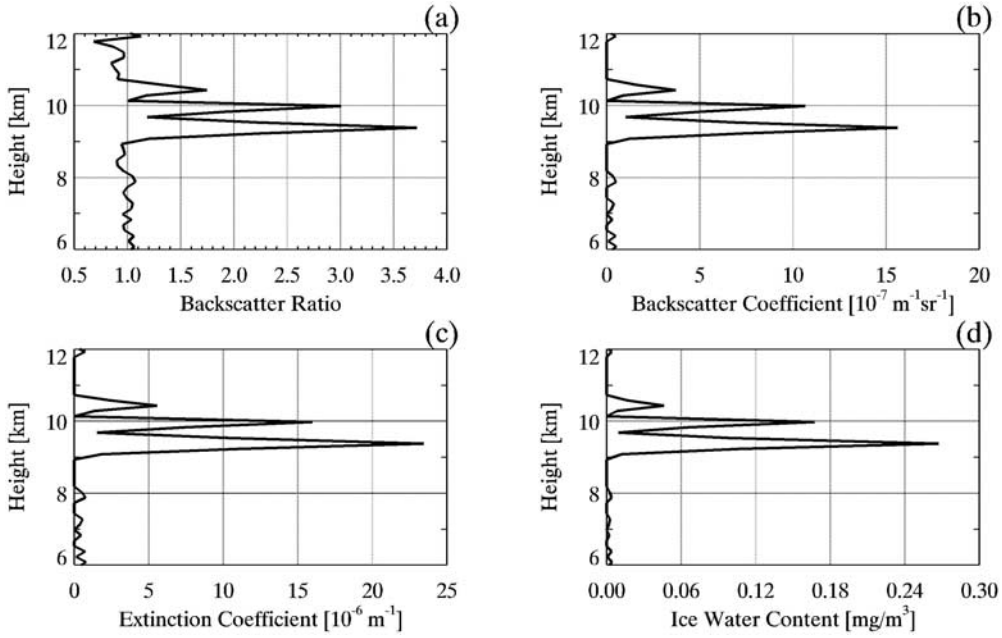


**Figure 6.** Four steps in the analysis of lidar data applied to the cloud backscatter signal in Figure 4.

expected that such thin water ice clouds will be detected in the atmosphere of Mars during the Phoenix mission [*Clancy et al.*, 1996; *Montmessin et al.*, 2004; *Pathak et al.*, 2008].

[17] Below a height of 2 km there is a reduction in the recorded photon counting signals in comparison with the expected molecular backscatter signal. This is caused by photon counting saturation due to electrical pulse overlap at high count rates. For the Phoenix lidar the nonlinear response occurs for count rates greater than 4 MHz. This has been characterized and can be corrected when there is not substantial variability within the averaging period [*Donovan et al.*, 1993]. However, there is no saturation in the signal recorded by analog to digital conversion.

[18] Figure 5 shows the 532 nm signal recorded by amplitude to digital conversion (ADC). The ratio of the Phoenix lidar to the York Lidar signals is constant with height above about 400m. The difference below 400 m is due to incomplete overlap between the outgoing laser pulse and the receiver FOV. This is consistent with the geometry of the system: the 12 cm separation between the telescope axis and the transmitter output, the 1.5 mrad FOV (side to side), the 0.5 mrad divergence, and the 0.2 mrad tilt of the transmitter output away from the telescope axis that occurs at a chassis temperature of $-30°$C. At this temperature there is complete transmitter-receiver overlap above 400 m.

## 4. Data Analysis

[19] The equation that describes a Lidar backscatter signal as a function of height can be written as

$$S(z) = C \times \beta(z) \times 1/z^2 \times T(z)^2 (\mathrm{MHz}).$$

$\beta(z)$ is the lidar backscatter coefficient and this represents the fraction of optical energy scattered back into the lidar receiver per unit length and per unit solid angle. T(z) is the transmittance through the atmosphere. This can be expressed in terms of optical thickness as $T = \exp(-\tau)$. The optical thickness is expressed in terms of the extinction coefficient as $\tau = \int \alpha \, dz$. The lidar equation has two parameters, $\beta$ and $\alpha$, that relate to the properties of material in the atmosphere. The derivation of extinction coefficient from lidar measurements is based on the method of *Fernald* [1984].

[20] The constant $C$ takes into account factors that include the laser pulse energy, area of the receiver aperture, transmittance of the receiver optics, and the quantum efficiency of the PMT detector in photon counting mode. This has been determined to have a value of $4 \times 10^{12}$ MHz m$^3$ by comparing the recorded backscatter signal to what is expected from the atmosphere based on measurement data from weather balloons (radiosondes). The lidar signal calculated for molecular backscatter only is shown in Figure 4 and this matches the measured signal where there is no cloud.

[21] In Figure 4, the average of the ratio of the signal above the cloud to the calculated molecular backscatter signal is 0.9. The reduction from a value of unity below the cloud is due to the attenuation through the cloud. Thus the two-way transmittance through the cloud is 0.9. From this value the optical depth of the cloud is determined to be 0.05. Multiple scattering will not be a significant factor in such an optically thin cloud with a receiver FOV of only 1.5 mrad [*Wandinger*, 1998]. The single scattering assumption in the lidar equation is valid for our purposes here.

[22] Figure 6 illustrates four steps in the analysis of lidar signals and the estimation of ice water content. This is making use of the lidar measurements of the cirrus cloud shown in Figure 4. Figure 6a is the ratio of the recorded backscatter to the calculated molecular backscatter. This is

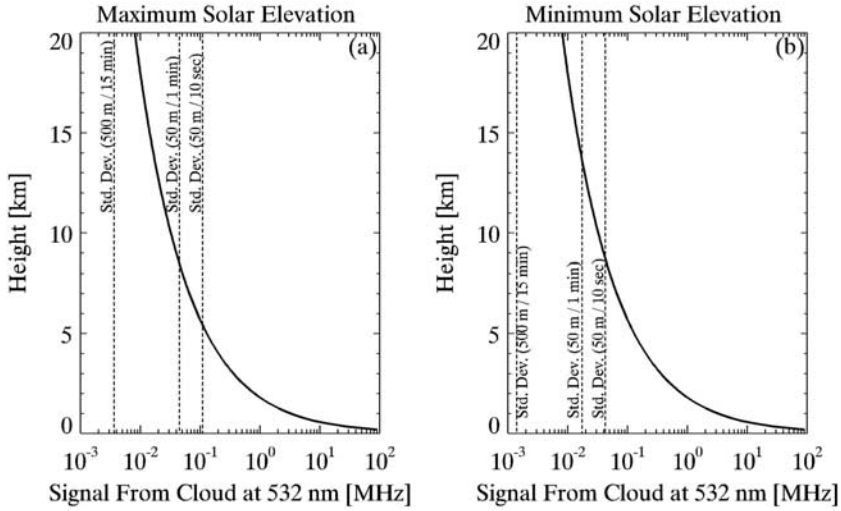


**Figure 7.** The 532 nm photon counting backscatter signal from a cloud equivalent to the one in Figure 4 (solid) compared with the standard deviation of the statistical fluctuation in the background skylight signal (dashed).

referred to as the attenuated backscatter ratio since the effect of extinction has not been taken into account. The cloud backscatter coefficients can be estimated from the backscatter ratio since the molecular backscatter coefficient is well known, and this is shown in Figure 6b. The retrieval of cloud extinction coefficient by the method of *Fernald* [1984] is shown in Figure 6c.

[23] The extinction coefficient can be expressed as the average effective cross-sectional area of the cloud ice crystals multiplied by the volume number density. This can also be considered as the total cross-sectional area of ice crystals per unit volume. If the relationship between area and volume is known for the ice crystals then one can determine the mass of water ice per unit volume, the ice water content (IWC). *Heymsfield et al.* [2005] have analyzed aircraft in situ measurements of cirrus cloud ice crystals to derive an empirical relationship between the extinction coefficient and the corresponding IWC. Figure 6d shows the IWC calculated from the extinction coefficient profile in Figure 6c, using the parameterization of *Heymsfield et al.* [2005].

[24] The capability to derive IWC from the lidar measurements on Mars will be of vital importance for investigating the transport of water through the atmosphere. One challenge in the analysis of the measurements from Mars is that the clouds will be in a dusty atmosphere and the background molecular atmosphere cannot be used as a reference as in Figure 4. There is also uncertainty in the assumption that the ice crystals in clouds observed by the lidar on Mars will be similar in size to ice crystals in the terrestrial cirrus clouds that were used to develop the parameterization. The parameterization can be adjusted for smaller ice crystals if necessary. However, numerical simulations [*Montmessin et al.*, 2004] of water ice clouds above the north polar region of Mars in summer do not indicate that the effective radius of the ice crystals will be substantially different from terrestrial cirrus clouds (e.g., on the order of 10 $\mu$m). Investigations are ongoing involving simultaneous lidar and aircraft in situ measurements in order to refine the parameterization and to quantify the uncertainty in deriving cloud IWC from lidar measurements in a dusty atmosphere such as Mars.

## 5. Lidar Performance Characteristics

[25] The performance of the Phoenix Lidar will be demonstrated here in terms of its ability to detect water ice clouds. The design requirement in this respect states that the lidar must be capable of detecting a cloud of optical thickness 0.05 at a height of 20 km when the dust at lower heights has an optical thickness of 0.2. It is fortuitous that the cirrus cloud at heights between 9 km and 11 km in Figure 4 has an optical depth of 0.05 (section 4). The lidar equation (section 4) was used to calculate the peak signal from a cloud with equivalent optical properties and geometrical thickness, situated at heights from ground to 20 km. It was assumed that dust below the cloud had an optical thickness of 0.2, regardless of the height of the cloud. This is shown in Figure 7.

### 5.1. Detection of Background Skylight

[26] The signal shown in Figure 4 was obtained just before 0500 LT during equinox at Ottawa and there was essentially zero background skylight detected within the 1 nm optical bandwidth of the Phoenix lidar. This will not be the case on Mars since the Phoenix mission will take place during the summer and the landing site will be at high latitude. The sun will be above the horizon for most of the mission. The background skylight will be the limiting factor and this must be taken into account in an assessment of the performance of the Phoenix lidar.

[27] The sensitivity of the Phoenix lidar to background skylight was determined by comparison with the background signal measured simultaneously with the York Lidar, which was previously calibrated. It was determined that the Phoenix lidar has a photon counting background skylight sensitivity of 0.4 MHz per unit of radiance in W m$^{-2}$ $\mu$m$^{-1}$ sr$^{-1}$.

[28] An atmospheric radiative transfer model [*Moores et al.*, 2007] has been applied to estimate the background light

intensity on the surface of Mars. With a dust optical thickness of 0.2 and at maximum solar elevation during the mission the background skylight intensity was estimated to be 10.2 in W $m^{-2}$ $\mu m^{-1}$ $sr^{-1}$. The skylight intensity at the minimum solar elevation that will be encountered during the mission was estimated to be 1.5 in W $m^{-2}$ $\mu m^{-1}$ $sr^{-1}$. The corresponding background count rates recorded by the Phoenix lidar are a maximum of 4.0 MHz and a minimum of 0.6 MHz.

### 5.2. Minimum Detectable Signal

[29] Photon counting will be used for detecting the very weak signals from high clouds. The minimum detectable signal level is determined by the statistical fluctuations (or uncertainty) inherent in the photon counting process. The statistical nature of Photon counting is described by the Poisson distribution in which the standard deviation is equal to the square root of the mean value. The magnitude of this statistical noise in the recorded signal will be determined by the background light level. The signal from clouds must be greater than the standard deviation of the statistical fluctuations (or uncertainty) in the background in order to be detectable.

[30] The standard deviation in the background count rate is shown in Figure 7 for temporal/spatial integrations of 15 min/500 m, 1 min/50 m, and 10 s/50 m. Figure 7a shows the results for maximum solar elevation, while Figure 7b shows the results for minimum solar elevation. It is seen that for maximum solar elevation the background standard deviation is about half of the peak signal from the cloud at 20 km when using the longest spatial/temporal averaging. The requirement for cloud detection up to 20 km is thus satisfied.

[31] The difference between midnight and midday measurements is also demonstrated in Figure 7. For temporal/spatial averaging of 1 min/50 m the cloud signal is equal to the background standard deviation at a height of 8.5 km at maximum solar elevation. At minimum solar elevation the cloud signal equals the statistical noise at a height of 13.5 km.

## 6. Conclusions

[32] The Phoenix mission to Mars will include the first lidar to be operated from the surface of a planet other than earth. This will observe the height distribution of atmospheric dust and clouds. These measurements will be combined with passive remote sensing and in situ measurements on board the spacecraft in order to investigate the weather and climate of the northern polar region of Mars.

[33] **Acknowledgments.** The Science Team for the Phoenix Lidar has been supported by the Canadian Space Agency (CSA) through contract 9F007–046053. An exceptional effort was provided by the engineering staff at MDA Space Missions during the instrument testing and the contributions of Andrew Kerr, Zul Dhanji, Ryan McCoubrey, Darren Hill, Lucas Clark, Mang Li, and Paul Roberts are thankfully acknowledged. The engineering staff from CSA played a key role, and we would especially like to acknowledge Rejean Fortier, Stephane Desjardins, Stephane Lapensee, and Isabelle Tremblay.

## References

Boynton, W. V., et al. (2002), Distribution of hydrogen in the near surface of Mars: Evidence for subsurface ice deposits, *Science*, *297*(5578), 81–85, doi:10.1126/science.1073722.

Clancy, R. T., A. W. Grossman, M. J. Wolff, P. B. James, D. J. Rudy, Y. N. Billawala, B. J. Sandor, S. W. Lee, and D. O. Muhleman (1996), Water vapour saturation at low altitudes around Mars aphelion: A key to Mars Climate?, *Icarus*, *122*, 36–62, doi:10.1006/icar.1996.0108.

Donovan, D. P., J. A. Whiteway, and A. I. Carswell (1993), Correction for nonlinear photon counting effects in lidar systems, *Appl. Opt.*, *32*, 6742–6753.

Fernald, F. G. (1984), Analysis of atmospheric lidar observations: Some comments, *Appl. Opt.*, *23*, 653–653.

Heymsfield, A. J., D. Winker, and G. van Zadelhoff (2005), Extinction-ice water content-effective radius algorithms for CALIPSO, *Geophys. Res. Lett.*, *32*, L10807, doi:10.1029/2005GL022742.

Leovy, C. (2001), Weather and climate on Mars, *Nature*, *412*, 245–249, doi:10.1038/35084192.

Measures, R. M. (1984), *Laser Remote Sensing: Fundamentals and Applications*, 510 pp., John Wiley, New York.

Montmessin, F., F. Forget, P. Rannou, M. Cabane, and R. M. Haberle (2004), The origin and role of water ice clouds in the Martian water cycle as inferred from a general circulation model, *J. Geophys. Res.*, *109*, E10004, doi:10.1029/2004JE002284.

Moores, J. E., P. H. Smith, R. Tanner, A. C. Schuerger, and K. J. Venkateswaran (2007), The shielding effect of small scale Martian surface geometry on ultraviolet flux, *Icarus*, *192*, 417–433, doi:10.1016/j.icarus.2007.07.003.

Neumann, G. A., D. E. Smith, and M. T. Zuber (2003), Two years of clouds detected by the Mars Orbiter Laser Altimeter, *J. Geophys. Res.*, *108*(E4), 5023, doi:10.1029/2002JE001849.

Newman, C. E., S. R. Lewis, and P. L. Read (2002), Modeling the Martian dust cycle: 1. Representations of dust transport processes, *J. Geophys. Res.*, *107*(E12), 5123, doi:10.1029/2002JE001910.

Pathak, J., D. Michelangeli, L. Komguem, J. A. Whiteway, and L. Tamppari (2008), Simulating Martian boundary layer water ice clouds and the lidar measurements for the Phoenix mission, *J. Geophys. Res.*, *113*, E00A05, doi:10.1029/2007JE002967.

Smith, P. H., et al. (2008), The Phoenix mission to Mars, *J. Geophys. Res.*, doi:10.1029/2008JE003083, in press.

Taylor, P. A., et al. (2008), Temperature, pressure and wind instrumentation on Phoenix MET, *J. Geophys. Res.*, doi:10.1029/2007JE003015, in press.

Wandinger, U. (1998), Multiple-scattering influence on extinction and backscatter coefficient measurements with Raman and high-spectral-resolution lidars, *Appl. Opt.*, *37*, 417–427, doi:10.1364/AO.37.000417.

A. Carswell, Optech Inc., 300 Interchange Way, Vaughan, ON L6S 4J3, Canada.

C. Cook, C. Dickinson, L. Komguem, and J. Whiteway, Department of Earth and Space Science and Engineering, York University, 4700 Keele Street, Toronto, ON M3J 1P3, Canada. (whiteway@yorku.ca)

M. Daly, MDA Space Missions, 9445 Airport Road, Brampton, ON L6S 4J3, Canada.

T. Duck, Department of Physics and Atmospheric Science, Dalhousie University, 6310 Coburg Road, Halifax, NS B3H 3J5, Canada.